2023 10th International Conference on Signal Processing and Integrated Networks (SPIN) | 978-1-6654-9099-3/23/$31.00 ©2023 IEEE | DOI: 10.1109/SPIN57001.2023.10116436

Experimental results from a proof-of-concept method for accurate volumetric estimation of hematoma in asymmetrically formed objects comprising solid materials as impediments.

Rahul Bhagawati
Dept. of Biosciences and Bioengineering (BSBE).
Indian Institute of Technology Guwahati.
North Guwahati, India.
r.bhagawati@iitg.ac.in

Souptick Chanda
Dept. of Biosciences and Bioengineering (BSBE).
Indian Institute of Technology Guwahati.
North Guwahati, India.
csouptick@iitg.ac.in

Cota Navin Gupta
Dept. of Biosciences and Bioengineering (BSBE).
Indian Institute of Technology Guwahati.
North Guwahati, India.
cngupta@iitg.ac.in

Suman Hazarika
Division of CT, MRI, and Conventional Radiology.
Apollo Hospitals, Guwahati.
sumanhazarika@rediffmail.com

***Abstract*— Hemorrhage, also known as internal bleeding, is a potentially fatal disorder requiring immediate medical attention based mainly on its seriousness. Medical imaging can qualitatively identify the extent of hemorrhage, but it is usually complicated to measure the amount of posthemorrhagic blood deposited inside the organs. Based on an imaging dataset, this study focuses on estimating blood volume with precision. A proof-of-concept (POC) phase has been designed for it. In Digital Imaging and Communications in Medicine (DICOM) format, images of liquid-filled vessels with irregular forms and hard, solid impediments inside them were obtained from computed tomography (CT) scans. These containers store various concentrations of aqueous iodine solution for our contrast CT scans. The estimated results of two novel volume quantification using slicing approaches and algorithms with minimum user input were designed, and they were contrasted with measurements of the liquid present.**

Keywords*— *hematoma, hemorrhage, CT scan, volume quantification, slicing method, voxel

I. INTRODUCTION

The degree of traumatic injuries can differ. Moreover, excessive bleeding from wounds calls for prompt attention and hospitalization because of its urgency. Blood volume constitutes approximately 7% of an adult's body weight, with an individual weighing 70 kg having an estimated blood volume (EBV) of 5 litres. When someone loses at least a litre of blood, an emergency blood transfusion is typically necessary within an hour [1]. If the hematoma volume is minimal, doctors may be able to stabilize the patient using medicine and saline solution. Precise blood hematoma quantification is crucial in such circumstances.

Quantifying hematoma from CT scans [2, 3] is essential in aiding clinicians in diagnosing and managing patients with internal bleeding. Hounsfield units (HU) are universally used in CT scanning to express CT numbers in a standardized and convenient form [4, 5]. Hounsfield units are derived from a linear transformation of the measured attenuation coefficients based on the densities of air and pure water, which are arbitrarily assigned:

1) the radiodensity of distilled water at standard temperature and pressure (STP) = 0 HU.
2) the radiodensity of air at STP = -1000 HU.

Brain hematoma is typically modest and consistent in shape, making it relatively easy to quantify. Brain haemorrhages range from 2 to 150 ml, in contrast to abdominal bleeding, which can reach up to hundreds and thousands of millilitres. The abdomen is highly irregular, with significant subject-specific variations, and clinical suspicion must be raised significantly in cases of traumatic abdominal blood loss. Hematemesis, haematuria, melena, and bruising are common signs and symptoms, with severe bleeding potentially resulting in haemorrhagic shock and death [6]. Therefore, quantifying blood or hematoma in such erratic spaces is challenging. A quantification method is necessary to establish the type of therapeutic aid, and blood volume required based on the amount of blood lost.

The slicing technique has been shown to be the most reliable and accurate method for quantifying hematoma volume in a CT slice computationally. The hematoma's form has no impact on it and it is resistant to errors resulting from uneven shape [7, 8, 9, 10]. The posthemorrhagic blood volume can be calculated using the slicing method as the sum of quantitative estimations from consecutive slices.

Our research aims to develop a therapeutically feasible software application that can accurately estimate blood volume in highly asymmetrical regions with non-overlapping HU regions with minimal inputs. A proof-of-concept (POC) study was undertaken to evaluate our approach's feasibility before commencing a larger-scale research project. This study was instrumental in identifying potential challenges and areas for improvement that need to be addressed before initiating the

actual study in subject-specific images of biological organs or bodily components.

Subsequent to proof-of-concept validation and clinical data analysis, the proposed software application is intended to possess the capability to detect and quantify patient bleeding expeditiously. This will enable healthcare professionals to receive prompt alerts and facilitate timely medical intervention. Additionally, the application aims to allow physicians to evaluate the characteristics and size of hematoma following a haemorrhagic stroke diagnosis. This will allow for appropriate treatment options and a more efficacious therapeutic approach.

II. Related work

Multiple techniques have been developed for measuring the volume of a hematoma, including the voxelization method, the slicing method, the Tada formula, region-based methods, and statistical models [11, 12, 13]. However, the Tada method is considered a rudimentary estimate and is ineffective in measuring asymmetrical hematomas. Region-based techniques like clustering (needs prior knowledge of the number of clusters) [14, 15], region-growing (seed-point accurate location is required to initiate) [16, 17, 18], contour-finding (do not give any information of its region) [19] and active contours (need to define the initiation point of the snake) [20, 21, 22, 23] have their limitations and challenges, making it sometimes difficult to obtain accurate segmentation. Training statistical models require large volumes of data and manual segmentation of CT scans, which is challenging due to variations in pixel intensity, borderlines, high-contrast tissues, noise, and aberrations. As research has shown, adequate visual examination and manual assessment of CT scans of hematomas require a lot of time, is vulnerable to intra- and inter-rater heterogeneity, and is prone to arbitrary inaccuracies and mischaracterizations [24].

III. Data

A. Data selection of the POC stage

For the POC portion of our research, we considered five containers with completely varied geometries in the context of data collection. These units held various concentrations of the aqueous iodine solution, allowing us to conduct contrast CT scans. Iodine solution is a high-density material that absorbs X-rays more strongly than surrounding tissue. This allows the iodine solution to appear as a bright white contrast agent in the resulting CT images, making it easier to distinguish different entities of the image [25].

The kind of container utilized for data collection, as well as the measured volume of aqueous iodine solution contained, are shown in Table I.

Table I: Utilized container type and volume measurements.

Container name	The measured volume of contrast solution (in ml)
[1] Blue small	100
[2] Blue small rugged	150
[3] Green MD	250
[4] Blue large flora	350
[5] Blue large BB	450

B. Interpretation of collected data

Two rounds of data gathering were used for the POC phase:

1) Varying concentrations of aqueous iodine solution inside each container. As seen in [26], this dataset has successfully completed the POC phase.
2) Varying concentrations of aqueous iodine solution and different numbers of impediments within every container.

It was essential to employ diverse container geometries to assess different primitives and establish the accuracy of volume estimations. To further strengthen the proposed algorithms' robustness, the incorporation of varying concentrations of iodine solution was strategically planned. This was particularly important given that the same CT scanner may yield varying Hounsfield unit values for identical tissues or entities, leading to patient-specific assessment discrepancies [27]. This phenomenon is evident in multiple bodily substances, including bones, blood, and peritoneal fluid, among others. Nonetheless, the final volume estimation was deemed sufficiently accurate and did not pose significant challenges.

Axial and frontal plane-specific CT images were obtained with the assistance of a skilled radiologist. In Fig. 1, examples of the scans in the axial view are shown, whereas, in Fig. 2, examples of the scans in the frontal view are shown. Five contrast-enhanced CT scans were performed, and more than 350 slices were captured in each image (in the axial plane).

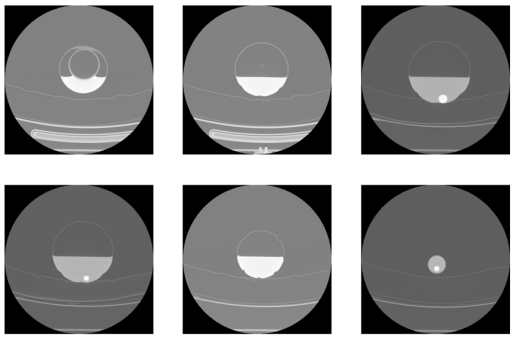

Fig. 1. Six CT segments of “Blue large BB” in axial view.

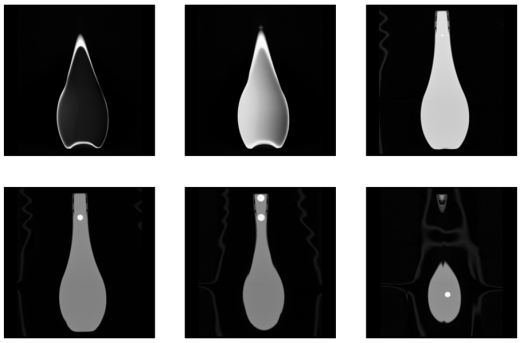

Fig. 2. Six CT segments of "Blue large BB" in frontal view.

IV. Methodology

The dataset was initially examined and analysed using the MicroDicom viewer 64-bit version (2022.1). It manages complete DICOM digital information, including pixel values and slice meta-information. The following measures were included in the entire process: background removal using thresholding segmentation, liquid region identification [28], and the equation for calculating the complete fluid volume (V) for a single 3D CT image is:

$$V = \sum ((l*b*h) * (pix)) \quad (1)$$

Here, the CT scan sampling rate is represented by the notation (l, b, h), and "pix" represents the total sum of segmented pixels in a single CT slice.

A. Algorithm-1

Based on a visual analysis of the CT slices using the MicroDicom viewer, Algorithm-1 selects a slice from a 3D CT-scan image having distinct views of the presence of both the liquid and the marbles. Four colourmaps were used for visualization and user input purposes. For each colourmap, the colourbar ticks are set to three different values. The users provided "liq_th" and "marb_th" as inputs for each colourbar tick. The lowest numerical value from the transformed HU values in the colourbar in the liquid-containing region is "liq_th", and the lowest numerical value from the transformed HU values in the colourbar in the solid/marbles-containing area is "marb_th". The individual mean value of "liq_th" and "marb_th" is determined from the list of inputs and used to segment all the slices. The sampling rate is computed and multiplied by the total number of foreground pixels. As a result, the volume of all the liquid present in one contrast-enhanced CT scan (vol_Sall or V) is determined using (1). Algorithm-1's flowchart is shown in Figure 3. The pseudo-code of Algorithm-1 is as follows:

1) Visualize and select a slice to identify the distinct presence of both liquid and marbles in it using the MicroDicom viewer.
2) For each selected CT slice:
   a. Use four proper colourmaps for visualization and user inputs.
   b. Set colourbar ticks to three values (say 100, 120, 150) for each colourmap.
   c. For each colourbar tick in each colourmap:
      i. Determine and obtain the lowest numerical value in the colourbar present in the liquid-containing region as "liq_th."
      ii. Determine and obtain the highest numerical value in the colourbar present in solid/marble-containing area as "marb_th."
3) Determine the individual mean value of "liq_th" and "marb_th" from the list of inputs.
4) Segment all slices using the mean value of "liq_th" and "marb_th."
5) Compute the sampling rate and multiply it by the total number of foreground pixels.
6) Determine the volume of all liquid present in one contrast-enhanced CT scan using formula (1).

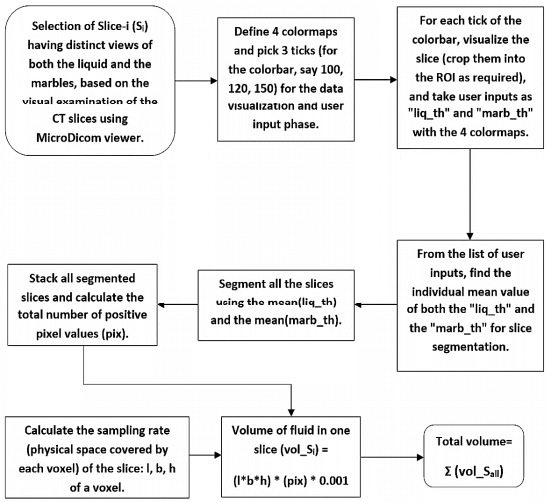

Fig. 3. Segmentation and volume estimation by algorithm-1.

B. Algorithm-2

Built on the user's input of a single pixel intensity value (th), Algorithm-2 is used. The liquid section's most frequent pixel intensity value is calculated by visual assessment of every CT slice. The slice values were divided by a "div size" value (say 15) based on the presence of the pixel value "th". Four colourmaps and four/five slices (containing both liquid and marbles) were chosen for visualization and user input. The users provided "liq_th" and "marb_th" as inputs for each colourbar tick, with the same meaning as the preceding algorithm. Minimum values of both "liq_th" and "marb_th" are determined from the list of inputs, respectively, and used to segment all the slices. The total number of foreground pixels is determined and multiplied by the element's sampling rate. Consequently, the entire liquid volume present in one contrast-enhanced CT image (vol_S_{all} or V) is determined by (1). Algorithm-2 is shown as a flowchart in Fig. 4. The pseudo-code of Algorithm-2 is as follows:

1) Calculate the most frequent pixel intensity value in the liquid section of each CT slice by visual assessment.

2) For each slice in 4-5 chosen slices (containing both liquid and marbles):
   a. Divide slice values by "div size" based on the presence of pixel value "th".
   b. For each of the 4 colourmaps:
      i. User provides "liq_th" and "marb_th" (meaning of both are the same as the previous algorithm) as inputs for each colorbar tick.
3) Determine minimum values of both "liq_th" and "marb_th" from the list of inputs.
4) Segment all the ROI-cropped slices using the determined minimum values.
5) Calculate the total number of foreground pixels.
6) Compute the sampling rate and multiply it by the total number of foreground pixels.
7) Determine the volume of all liquid present in one contrast-enhanced CT scan using formula (1).

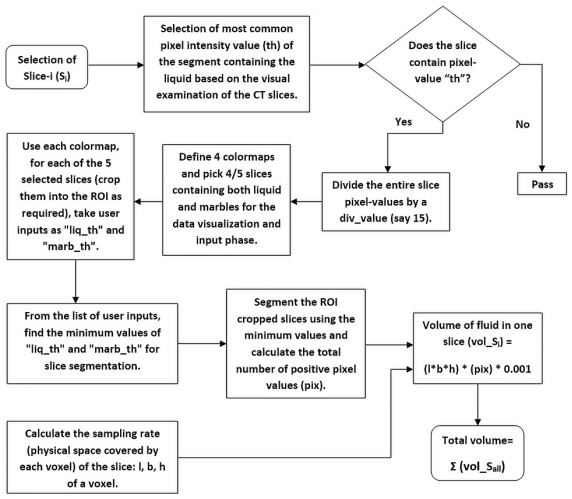

Fig. 4. Segmentation and volume estimation by algorithm-2.

V. Results and Discussion

We looked at five distinct liquid-carrying (aqueous iodine solution) containers with various capacities. The containers are shaped differently and asymmetrically. The segmentation and volume quantification tasks were performed on an AMD Ryzen 7 machine having a 2.3 GHz CPU running on Windows 11 and 16 GB of RAM. Algorithm-1 underestimated the volume of the first container, "Blue small," as seen in Table II. Contrarily, the volume of the other four containers was calculated more accurately, leading to the last container, “Blue large BB”, having the best volume estimate. However, for the first four containers, Algorithm-2 outscored Algorithm-1. Algorithm-2 produced the most accurate result for the fourth container, i.e., “Blue large flora”. The outputs or estimations from Algorithm-2 are displayed in Table III.

Table II: Volumes determined by Algorithm-1.

Container type	Measured volume (in ml) of contrast solution with marbles	Algorithm-1			
		Mean thresholds (liq_th, marb_th)		Calculated volume (in ml) with accuracy	
Blue small	100	383.33	2460	86.91	86.91%
Blue small rugged	150	384.17	2363.33	136.99	91.33%
Green MD	250	363.33	2240	233.82	93.53%
Blue large flora	350	593.33	2277.5	324.51	92.72%
Blue large BB	450	681.67	2185	435.47	96.77%

Table III: Volumes determined by Algorithm-2.

Container type	Measured volume (in ml) of contrast solution with marbles	Algorithm-2			
		Min thresholds (liq_th, marb_th)		Calculated volume (in ml) with accuracy	
Blue small	100	300	1800	89.78	89.78%
Blue small rugged	150	330	1725	140.17	93.45%
Green MD	250	300	1650	240.23	96.09%
Blue large flora	350	450	1650	339.30	96.94%
Blue large BB	450	675	1575	435.16	96.70%

As shown in Table IV, averaging the predicted volumes from Algorithms-1 and 2 resulted in a more balanced and consistent list of overall results for each container. However, it is worth noting that this approach resulted in estimates that were somewhat less accurate than those produced by Algorithm-2.

Table IV: Values in bold signify most accurate volume estimates.

Container type	Measured volume (in ml) of contrast solution with marbles	Algorithm-1 estimated volume (in ml) with accuracy	Algorithm-2 estimated volume (in ml) and accuracy	Average volumes (in ml) by Algorithms 1 and 2 with accuracy
Blue small	100	86.91 (86.91%)	**89.78 (89.78%)**	88.35 (88.35%)
Blue small rugged	150	136.99 (91.33%)	**140.17 (93.45%)**	138.58 (92.39%)
Green MD	250	233.82 (93.53%)	**240.23 (96.09%)**	237.03 (94.81%)
Blue large flora	350	324.51 (92.72%)	**339.30 (96.94%)**	331.91 (94.83%)
Blue large BB	450	**435.47 (96.77%)**	435.16 (96.70%)	435.32 (96.74%)

The computational complexity of each algorithm, as measured by the time taken, is as follows:

1) Algorithm-1 visualised a single slice containing both liquid and marbles, 4 colormaps per slice, and 3 colorticks per colormap. There was a total of 24 similar inputs integrated, 12 for "liq_th" and 12 for "marb_th." Input process took 2-3 minutes, while thresholding and quantification took less than 10 seconds.
2) Algorithm-2 was divided into 4 slices, each with 4 colormaps. There were 32 similar inputs used in total, 16 for "liq_th" and 16 for "marb_th." Input process took 2-3 minutes, while thresholding and quantification took less than 10 seconds.

The two algorithms require minimal user inputs and have the advantage of efficiently handling such datasets (with non-overlapping HU regions). Algorithm-2 almost outperformed Algorithm-1 due to its integration of visualisation and input data derived from 4-5 distinct slices containing both liquid and marbles. In contrast to Algorithm-1, Algorithm-2 used the minimum values of "liq_th" and "marb_th" from the input list. The use of the minimum inputs by Algorithm-2 is believed to have aided in the identification of non-overlapping regions of contrast liquid and marbles with greater precision.

The two algorithms' efficiency in our dataset is due to two key factors: effective visualisation and localization of ROIs in each slice of the dataset, and distinct separation of HU values in each CT slice. These factors helped to identify and isolate ROIs using simple visual inspection. The algorithms are designed to reduce the additional expertise required to execute specific sophisticated models. Algorithm-2 is a better choice than Algorithm-1 for quantifying hematomas in highly asymmetrical regions. However, there are some issues that must be addressed. The regions must, in particular, have non-overlapping HU regions, such as contrast-enhanced regions, and clear visuals of their ROIs. While the segmentation and volume estimation tasks appear promising for both algorithms, more research is needed to determine their accuracy and reliability in different hematoma shapes and sizes.

VI. Conclusion

Accurate hematoma volume measurement is critical for effective clinical decision-making, prognosis, and treatment of traumatic brain injury patients. Though many techniques for measuring hematoma volume have been developed, each has advantages and limitations. The effective approach depends on the characteristics of the hematoma and the available resources.

The new algorithms, particularly Algorithm-2, have the potential to improve clinical decision-making and patient outcomes significantly. To overcome the limitations of manual segmentation, such as high variability and error susceptibility, it is also necessary to modify and improve the algorithms and test them in clinical images. A "test and tune" process can assist in identifying and correcting any potential inaccuracies in the output of the algorithms, ensuring that the results are accurate and reliable. Hence, medical imaging-based assessments are necessary to establish the effectiveness of these algorithms in estimating hematoma and treating patients with traumatic injuries.

VII. Prospects for Further Research

The following future scope of work is anticipated based on the findings of the POC phase mentioned above:

1) The novel algorithms will be subjected to clinical data trials and testing.
2) Semi-supervised superpixel segmentation techniques will be used to segregate the acquired data into more relevant sections [29].
3) Voxel masks will be created and neural networks will be trained on these masks to construct probability mappings for each slice of the targeted pixels, thus enabling automated voxel labelling [11].
4) A hierarchical evolutionary algorithm will be employed to segment fluid from other bodily materials, and the slicing approach will be adopted to measure volume [30].

VIII. Authors' contributions

These are the authors' contributions to the study: Rahul Bhagawati, Souptick Chanda, and Cota Navin Gupta created and wrote the document. It was done after Rahul Bhagawati and Suman Hazarika conceptualized and conducted the research, gathered the data, and analysed and interpreted the findings. The concluding form of the paper was confirmed after all the authors evaluated the results.

IX. References

[1] G. Gutierrez, H. D. Reines, and M. E. Wulf-Gutierrez, "Clinical review: hemorrhagic shock," Crit. Care, vol. 8, no. 5, pp. 373–381, 2004.

[2] "What is a CT scan?," WebMD. [Online]. Available: https://www.webmd.com/cancer/what-is-a-ct-scan. [Accessed: 30-Mar-2023].
[3] Wikipedia contributors, "CT scan," Wikipedia, The Free Encyclopedia, 02-Mar-2023. [Online]. Available: https://en.wikipedia.org/w/index.php?title=CT_scan&oldid=1142432791.
[4] B. Vanderstraeten, N. Johnston, and J. Ketelaars, "PO-1493 Comparison of CBCT Hounsfield Unit to density conversion methods for treatment plan evaluation," Radiother. Oncol., vol. 170, pp. S1269–S1270, 2022.
[5] D. Bell and K. Greenway, "Hounsfield unit," Radiopaedia.org. Radiopaedia.org, 09-Jul-2015.
[6] A. B. Johnson and B. Burns, Hemorrhage. StatPearls Publishing, 2023.
[7] M. Chen, Z. Li, J. Ding, X. Lu, Y. Cheng, and J. Lin, "Comparison of common methods for precision volume measurement of hematoma," Comput. Math. Methods Med., vol. 2020, p. 6930836, 2020.
[8] Z. Jingjing et al., "Pretreatment of sulfonylureas reducing perihematomal edema in diabetic patients with basal ganglia hemorrhage: A retrospective case-control study," Front. Neurol., vol. 12, p. 736383, 2021.
[9] J. Egger, T. Kapur, C. Nimsky, and R. Kikinis, "Pituitary adenoma volumetry with 3D Slicer," PLoS One, vol. 7, no. 12, p. e51788, 2012.
[10] E. R. Velazquez et al., "Volumetric CT-based segmentation of NSCLC using 3D-Slicer," Sci. Rep., vol. 3, no. 1, p. 3529, 2013.
[11] R. Dhar et al., "Deep learning for automated measurement of hemorrhage and perihematomal edema in supratentorial intracerebral hemorrhage," Stroke, vol. 51, no. 2, pp. 648–651, 2020.
[12] N. Ironside et al., "Fully automated segmentation algorithm for hematoma volumetric analysis in spontaneous intracerebral hemorrhage," Stroke, vol. 50, no. 12, pp. 3416–3423, 2019.
[13] A. Arab et al., "A fast and fully-automated deep-learning approach for accurate hemorrhage segmentation and volume quantification in non-contrast whole-head CT," Sci. Rep., vol. 10, no. 1, p. 19389, 2020.
[14] Wikipedia contributors, "Cluster analysis," Wikipedia, The Free Encyclopedia, 14-Feb-2023. [Online]. Available: https://en.wikipedia.org/w/index.php?title=Cluster_analysis&oldid=1139362353.
[15] "Clustering in machine learning," GeeksforGeeks, 15-Jan-2018. [Online]. Available: https://www.geeksforgeeks.org/clustering-in-machine-learning/. [Accessed: 30-Mar-2023].
[16] Wikipedia contributors, "Region growing," Wikipedia, The Free Encyclopedia, 30-Nov-2022. [Online]. Available: https://en.wikipedia.org/w/index.php?title=Region_growing&oldid=1124749382.
[17] S. A. Hojjatoleslami and J. Kittler, "Region growing: a new approach," IEEE Trans. Image Process., vol. 7, no. 7, pp. 1079–1084, 1998.
[18] R. Adams and L. Bischof, "Seeded region growing," IEEE Trans. Pattern Anal. Mach. Intell., vol. 16, no. 6, pp. 641–647, 1994.
[19] "Contour finding — skimage v0.20.0 docs," Scikit-image.org. [Online]. Available: https://scikit-image.org/docs/stable/auto_examples/edges/plot_contours.html. [Accessed: 30-Mar-2023].
[20] Wikipedia contributors, "Active contour model," Wikipedia, The Free Encyclopedia, 25-Jun-2022. [Online]. Available: https://en.wikipedia.org/w/index.php?title=Active_contour_model&oldid=1094961149.
[21] D. Bhatt, "Active contours - A method for image segmentation in computer vision," Analytics Vidhya, 13-Sep-2021. [Online]. Available: https://www.analyticsvidhya.com/blog/2021/09/active-contours-a-method-for-image-segmentation-in-computer-vision. [Accessed: 30-Mar-2023].
[22] R. J. Hemalatha, T. R. Thamizhvani, A. J. A. Dhivya, J. E. Joseph, B. Babu, and R. Chandrasekaran, "Active contour based segmentation techniques for medical image analysis," in Medical and Biological Image Analysis, InTech, 2018.
[23] H.-X. Liu, J.-X. Fang, Z.-J. Zhang, and Y.-C. Lin, " Localised edge‐region‐based active contour for medical image segmentation," IET Image Process., vol. 15, no. 7, pp. 1567‐1582, 2021.
[24] V. V et al., "Automated detection and screening of traumatic brain injury (TBI) using computed tomography images: A comprehensive review and future perspectives," Int. J. Environ. Res. Public Health, vol. 18, no. 12, p. 6499, 2021.
[25] "Iodine-containing contrast medium," InsideRadiology, 13-Sep-2016. [Online]. Available: https://www.insideradiology.com.au/iodine-containing-contrast-medium. [Accessed: 30-Mar-2023].
[26] R. Bhagawati, S. Hazarika, C. N. Gupta, and S. Chanda, "Precise volumetric quantification of blood (hematoma) in deformable solids/organs: preliminary results based on a proof-of-concept scheme," in 2021 International Conference on Electrical, Computer and Energy Technologies (ICECET), 2021.
[27] R. Lamba et al., "CT Hounsfield numbers of soft tissues on unenhanced abdominal CT scans: variability between two different manufacturers' MDCT scanners," AJR Am. J. Roentgenol., vol. 203, no. 5, pp. 1013–1020, 2014.
[28] H. Sun and H. Sun, "A novel measure method of cerebral hematoma volume," Interdiscip. Neurosurg., vol. 14, pp. 42–46, 2018.
[29] H. Yao, C. Williamson, J. Gryak, and K. Najarian, "Brain hematoma segmentation using active learning and an active contour model," in Bioinformatics and Biomedical Engineering, Cham: Springer International Publishing, 2019, pp. 385–396.
[30] B. Liu, Q. Yuan, Z. Liu, X. Li, and X. Yin, "Automatic segmentation of intracranial hematoma and volume measurement," Annu. Int. Conf. IEEE Eng. Med. Biol. Soc., vol. 2008, pp. 1214–1217, 2008.